

Triplet Excitations in Carbon Nanostructures

K. Aryanpour,¹ S. Mazumdar,^{1,2} and H. Zhao³

¹*Department of Physics, University of Arizona, Tucson, Arizona 85721, USA*

²*College of Optical Sciences, University of Arizona, Tucson, Arizona 85721, USA*

³*School of Physics and Telecommunication Engineering,
South China Normal University, Guangzhou, China*

(Dated: September 19, 2021)

We show that the energy differences between the lowest optical singlet exciton and the lowest triplet exciton in semiconducting single-walled carbon nanotubes with diameter ~ 1 nm and graphene nanoribbons with widths ~ 2 nm are an order of magnitude smaller than in the π -conjugated polymer poly(para-phenylenevinylene). Our calculated energy gaps between the singlet and triplet excitons are in excellent agreement with the measured values in three different nanotubes with diameters close to 1 nm. The spatial extent of the triplet exciton is nearly the same as that of the singlet exciton in wide nanotubes and nanoribbons, in contrast to that in π -conjugated polymers, in which the triplet exciton exhibits strong spatial confinement. Weakly confined behavior of the triplet state begins in nanoribbons with widths as narrow as 2.5 times the graphene unit lattice vector. We discuss possible consequences of the small singlet-triplet energy difference in the carbon nanostructures on device applications.

I. INTRODUCTION

Although the spin-singlet excitations in semiconducting single-walled carbon nanotubes (S-SWCNTs) have been widely investigated both theoretically and experimentally¹, the literature on spin-triplet excitations in these systems is relatively sparse. Theoretical predictions of the energy difference between the optically bright spin-singlet exciton and the lowest triplet exciton (hereafter Δ_{ST}) in the S-SWCNTs vary widely, with estimates of Δ_{ST} in S-SWCNTs with diameter $d \sim 1$ nm ranging from $\sim 20 - 40^{2,3}$ to ~ 300 meV⁴. The earliest determination of spin triplet excitations were for S-SWCNTs with large $d \sim 1.4 - 1.8$ nm, where Δ_{ST} are rather small⁵ and precise calculations are difficult. Experimental identification of triplet excitations is made difficult by the occurrence of optically dark spin-singlet excitons below the singlet bright exciton⁶⁻¹². It is significant, however, that early experimental work on S-SWCNTs with $d \sim 1$ nm found two distinct groups of optically dark excitons⁹, redshifted relative to the singlet bright exciton by ~ 40 meV and 100-130 meV, respectively, a point we come back to later. More recent careful measurements have determined the energy locations of the lowest triplet excitons in several S-SWCNTs with diameters close to 1 nm¹³⁻¹⁵. The experimental Δ_{ST} are different from both sets of theoretical predictions and are intermediate in magnitude (see below). In contrast to nanotubes, where considerable photophysical studies have been carried out, the existing literature on the photophysics of graphene nanoribbons (GNRs) is largely theoretical in nature¹⁶⁻²⁰. Discussions here

have been limited to spin-singlet excitations only.

The sparseness of the literature on triplet excitations is surprising, since even though the spin-selection rule requires that optical excitations from the singlet ground state occur only to singlet excited states, triplet excitations can play strong indirect roles in optoelectronic applications. In the context of light emitting diodes with molecular or polymeric π -conjugated systems as the active materials, for example, the relative yields of light emissive singlet excitons versus nonemissive triplet excitons in electroluminescence is a topic of strong interest²¹⁻²⁷. The formation rates of the singlet and triplet excitons depend strongly on Δ_{ST} ^{23,24}. Similar discussions are ongoing also in the area of organic photovoltaics; the possibility of harvesting longlived triplet excitons that are reached from the singlet optical exciton via *intersystem crossing* (ISC)²⁸ or *singlet fission*²⁹ are being actively investigated. The efficiencies of both ISC and fission depend on Δ_{ST} . Thorough investigation of Δ_{ST} and the nature of the spin-triplet excitations in the carbon nanostructures is thus called for.

In the present paper, we report the results of theoretical calculations of triplet excitations in several S-SWCNTs and armchair GNRs (AGNRs) within a molecular correlated-electron model. We compare these results with those for poly(para-phenylenevinylene) (PPV) for which experimental results are known³⁰. Our findings reveal that there is a *qualitative* change in the triplet state wave function in AGNRs with increasing width; nanoribbons with widths as narrow as 2.5 times the graphene lattice vector already exhibit small Δ_{ST} . Coulomb correlation effects on the honeycomb lattice appear to

be different from those in one-dimensional chainlike systems. Similar behavior as AGNRs for the triplet state wave function is also found in S-SWCNTs with increasing diameter.

II. MODEL AND PARAMETERS

Our studies are within the correlated π electron Pariser-Parr-Pople (PPP) Hamiltonian^{31,32}. For PPV, accurate theoretical results for both singlet and triplet excitations have previously been obtained within the PPP Hamiltonian³³. The PPP model has also been used previously to investigate the spin singlet subspace in S-SWCNTs. For the longitudinal singlet excitons seen in optical absorption measurements with light polarized parallel to the nanotube axes, nearly quantitative fits to experimental absolute exciton energies and exciton binding energies have been obtained for nanotubes with diameter $d \geq 0.75$ nm³⁴. Quantitatively accurate energies have also been obtained for the transverse excitons seen in absorption experiments with light polarized transverse to the nanotube axes³⁵. Similar accuracies are expected for the spin triplet subspace within the model.

We write the PPP Hamiltonian as,

$$H = - \sum_{\langle ij \rangle, \sigma} t_{ij} (c_{i,\sigma}^\dagger c_{j,\sigma} + \text{H.c.}) + \sum_i U n_{i,\uparrow} n_{i,\downarrow} + \sum_{i < j} V_{ij} (n_i - 1)(n_j - 1). \quad (1)$$

where $c_{i,\sigma}^\dagger$ creates a π electron of spin σ on carbon atom i , $n_{\mu,\sigma} = c_{i,\sigma}^\dagger c_{i,\sigma}$, and $n_i = \sum_\sigma n_{i,\sigma}$. We restrict the one-electron hopping t_{ij} to nearest neighbors without loss of generality³⁵. U is the repulsion between two electrons occupying the same p_z orbital of a C atom and V_{ij} are intersite Coulomb interactions.

Our choice of the t_{ij} is system dependent. For PPV, we assume a planar configuration and choose $t_{ij} = 2.4$ eV for phenyl C-C bonds and 2.2 (2.6) eV for the single (double) C-C bonds of the vinylene group³³. We assume hydrogenation of the edge carbon atoms in AGNRs and take uniform $t_{ij} = 2.4$ eV. In real systems, the site energies of the edge carbon atoms and hopping integrals linking them are expected to be slightly different from the corresponding quantities for the carbon atoms near the centers of the nanoribbons. However, we expect this effect to contribute weakly to the relatively large difference in Δ_{ST} between PPV and AGNRs (see below). For the S-SWCNTs, based on earlier work,³⁴ we set

$t_{ij} = 2.0$ eV. The curved nature of the S-SWCNT surface calls for the smaller value³⁴.

The onsite Coulomb interaction U is obviously identical for all three families. The intersite Coulomb interactions are parametrized as $V_{ij} = U/(\kappa\sqrt{1 + 0.6117R_{ij}^2})$, where R_{ij} is the distance between C atoms i and j in Angstroms. In the above expression, $\kappa = 1$, with $U = 11.26$ eV correspond to the standard Ohno parametrization³⁶ for the PPP model. Considerably better fits to experiments are obtained with slightly smaller U and large κ . Based on the fitting of ground state as well as excited state absorptions in PPV³³ and S-SWCNTs,^{34,35} we chose $U = 8.0$ eV and $\kappa = 2$.

The model systems we have chosen for our theoretical study are (i) a 20-unit PPV chain capped at both ends, (ii) S-SWCNTs characterized by indices $(n, m) = (8, 0)$, $(11, 0)$, $(6, 4)$, $(6, 5)$, $(7, 5)$, $(7, 6)$, and $(9, 4)$, and AGNRs, which we describe with the labeling scheme of Ezawa³⁷: $(p, q) = (15, 1)$, $(19, 1)$, and $(21, 1)$. The zigzag S-SWCNTs were chosen because of the simplicity of performing calculations for these with a very large number of unit cells. Previous experience has shown that energy difference in nanotubes depend primarily on diameters d and relatively weakly on chiralities. Thus the calculated Δ_{ST} for the zigzag nanotubes may be considered representative for all nanotubes with diameters that are close. In contrast to the zigzag S-SWCNTs, experimental results for Δ_{ST} are available for the $(6, 4)$, $(7, 5)$, and $(9, 4)$ nanotubes. We show below that our calculated results for both the spin-singlet bright exciton and the lowest spin-triplet exciton are in excellent agreement with experiments in these cases. While the triplet subspace of the two remaining chiral S-SWCNTs in our list, $(6, 5)$ and $(7, 6)$, have not been studied experimentally yet, their photophysics has been widely investigated in the past. The long exciton lifetime in the $(6, 5)$ S-SWCNT has allowed experimental estimation of the size and the mobility of the optical singlet exciton³⁸. Our calculated singlet exciton size compares very favorably with the experimental value. Our predicted theoretical results for triplet excitations can thus be compared against future experiments in the $(6, 5)$ and $(7, 6)$ S-SWCNTs. The AGNRs we have chosen are obtained by unrolling our zigzag nanotubes after cutting them along their translational vectors.

As in previous works^{34,35}, our calculations for the S-SWCNTs and AGNRs are done with open boundary condition. For the zigzag S-SWCNTs, our calculations are for 50 unit cells with ~ 2000 carbon atoms in each case. For the chiral S-SWCNTs the number of unit cells we retain is smaller, but the number of

carbon atoms is comparable; in all cases, we retain larger than 2000 carbon atoms. Furthermore, for each of the three S-SWCNTs for which experimental results are available, we have done careful finite-size analysis to confirm that our calculated energies have converged to within a few percent. Calculations for the AGNRs are for 40 unit cells.

Tractable approximate approaches to the many-body PPP Hamiltonian are necessary to determine the excitation energies of large systems. As discussed in the context of singlet excitations^{34,35}, we use the single configuration interaction (SCI) approximation, which involves diagonalization of the PPP Hamiltonian in the space of single excitations from the Hartree-Fock (HF) ground state. The excitation of a single electron from the ground state can give either the singlet or triplet electron-hole pair or exciton. Indirect exchange within Eq. (1) differentiates between the two spin states.

III. RESULTS AND DISCUSSIONS

In Table I, we have given our calculated singlet and triplet exciton energies (hereafter E_S and E_T , respectively). In the case of the S-SWCNTs, there occur singlet dark excitons below the optical bright exciton. We have found that similar structures, with several close-lying triplet states, occur also in the spin triplet subspace. In Table I, E_S corresponds to the singlet bright exciton and E_T to the *lowest* triplet exciton. Thus in S-SWCNTs, there occur several dark singlet and triplet excitons between these two states. We have also included in Table I the calculated singlet exciton binding energies (hereafter E_{bS}), corresponding to the difference in energy between the lowest HF continuum within SCI and the singlet exciton³⁴. Quantitative agreement between the calculated E_S and E_{bS} , and their experimental estimates³⁹⁻⁴¹ in S-SWCNTs have been pointed out earlier³⁴. We therefore compare theory and experiments here only for the S-SWCNTs for which triplet energies are available. For PPV, the calculated $E_S = 2.69$, $E_T = 1.46$, and $\Delta_{ST} = 1.23$ eV are to be compared against experimental quantities 2.4, 1.3, and 1.1 eV, respectively³⁰. The experimental triplet exciton energies for the (6, 4), (7, 5), (9, 4) S-SWCNTs in Table I were obtained from emissions from triplet states that became optically active upon pulsed-laser irradiation^{13,15} or hydrogen absorption¹⁴. It is reasonable to assume that the emissions are from the lowest triplet exciton within the triplet manifold¹³⁻¹⁵. Excellent agreement between theory and experiments is seen in all three cases. The most striking aspect of the results in Ta-

System			E_S (eV)	E_T (eV)	Δ_{ST} (eV)	E_{bS} (eV)
PPV (20 units)			2.69	1.46	1.23	0.85
SWCNT	(n, m)	d (nm)				
	(8,0)	0.64	1.44	1.28	0.16	0.56
	(6,4)	0.69	1.33 (1.42 ^a)	1.22 (1.29 ^b)	0.11 (0.13)	0.50 (0.49 ^c)
	(6,5)	0.76	1.24	1.14	0.10	0.46
	(10,0)	0.79	1.18	1.08	0.10	0.43
	(7,5)	0.83	1.15 (1.21 ^a)	1.07 (1.10 ^d)	0.08 (0.11)	0.43 (0.39 ^c)
	(11,0)	0.87	1.11	1.00	0.11	0.41
	(7,6)	0.90	1.08	0.99	0.09	0.39
	(9,4)	0.91	1.06 (1.13 ^a)	0.98 (1.02 ^d)	0.08 (0.11)	0.39 (0.34 ^c)
GNR	(p, q)	w (nm)				
	(15,1)	1.98	0.90	0.82	0.08	0.32
	(19,1)	2.49	0.74	0.67	0.06	0.28
	(21,1)	2.73	0.77	0.70	0.07	0.26

^a From Ref. 41. ^b From Ref. 13. ^c From Ref. 39. ^d From Ref. 15.

TABLE I: Calculated singlet and triplet exciton energies E_S and E_T , the singlet-triplet energy difference Δ_{ST} , and the singlet exciton binding energy E_{bS} , in PPV, S-SWCNTs and AGNRs. Experimental values from Refs. 13, 15, 39 and 41 are given in parentheses.

(6,4)			(7,5)			(9,4)		
L (N)	E_S (eV)	E_T (eV)	L (N)	E_S (eV)	E_T (eV)	L (N)	E_S (eV)	E_T (eV)
8 (1216)	1.345	1.195	2 (872)	1.174	1.063	2 (1064)	1.173	0.979
10 (1520)	1.338	1.204	3 (1308)	1.153	1.062	3 (1596)	1.090	0.975
12 (1824)	1.334	1.211	4 (1744)	1.148	1.069	4 (2128)	1.065	0.978
14 (2128)	1.332	1.218	5 (2180)	1.145	1.071			

TABLE II: Convergence behavior of E_S and E_T for (6, 4), (7, 5) and (9, 4) S-SWCNTs with increasing length. Here L (N) is the number of unit cells (total number of carbon atoms).

ble I is the very small Δ_{ST} in the S-SWCNTs and the AGNRs, nearly one order of magnitude smaller than that in PPV. We do not find the simple A/d^2 diameter dependence of Δ_{ST} suggested previously³.

For each of the chiral S-SWCNTs in Table I, our results are for the longest nanotubes that were computationally accessible. Whether or not convergence in energies has been reached is clearly an important issue, both from the perspective of comparisons to experiments and because of the seemingly surprising difference between S-SWCNTs and PPV in the triplet sector, given that in the singlet sector E_{bS} in S-SWCNTs is smaller than that of PPV by only about a factor of 2. We have therefore done careful finite-size analysis for the three S-SWCNTs for which experimental results are available for both the singlet bright exciton and the triplet exciton. In Table II, we have shown these results. Convergence to a few percent or less in both E_S and E_T gives

our confidence about our results in Table I. Comparing our results for the (7,6) S-SWCNT with that in Ref. 4, we see that the reason for the large Δ_{ST} found in that work lied not in the limitation to two unit cells, but the relatively large difference between the calculated spin-singlet exciton energy there and the experimental value.

In order to understand physically the origin of the difference between PPV on the one hand and S-SWCNTs and AGNRs on the other, we have done careful wave function analyses. The amplitude for an electron located at site i in real space with a hole located at site j within a bound electron-hole exciton is

$$A_{ij}^{S(T)} = \langle \Psi_{S(T)} | c_{i\uparrow}^\dagger c_{j\downarrow} \mp c_{i\downarrow}^\dagger c_{j\uparrow} | G \rangle \quad (2)$$

with $|\Psi_{S(T)}\rangle$ the SCI singlet (triplet) exciton wave function and $|G\rangle$ the HF ground-state wave function^{4,42}. In Eq. (2), the minus (plus) sign corresponds to the singlet (triplet) exciton. Figure 1 presents our results for the electron-hole spatial separation probability $\rho_{ij}^{S(T)} = |A_{ij}^{S(T)}|^2$ plotted versus carbon atoms i and j for the excitons of a 20-unit PPV chain (158 carbon atoms). Each point i on the diagonal gives the probability of finding the electron and the hole on the same location, and vertical displacements from the diagonal points i gives the probability of finding a hole at some $j \neq i$, with the electron fixed at i . Giving multiple i becomes necessary because of the open boundary condition we have chosen. Microscopic details such as electron-hole separations within a unit cell cannot be obtained from the figure, which, however, does give a coarse-grained comparison between singlet and triplet excitons.

Figure 1 indicates that the triplet exciton in PPV exhibits a significantly more localized probability density compared to the singlet exciton. This result has also been obtained previously by other investigators⁴³. For the triplet exciton in Fig. 1(b), the “hot spots” (atoms with high probability intensity colored in yellow and red according to the calibration column next to every density plot) are almost entirely along the diagonal, while for the singlet exciton in Fig. 1(a), hot spots are evenly distributed within the neighborhood of nearly 20 atoms about the diagonal. The root mean square (rms) electron-hole separation (“exciton size”) $d_{S(T)} = \sqrt{\sum_{ij} \rho_{ij}^{S(T)} \|\vec{R}_i - \vec{R}_j\|^2}$, where \vec{R}_i (\vec{R}_j) gives the location of the electron (hole), is thus significantly different for singlet and triplet excitons ($d_T/d_S \sim 0.5$, see Fig. 1). This *qualitative* difference between the spin singlet and triplet excitons in one dimension

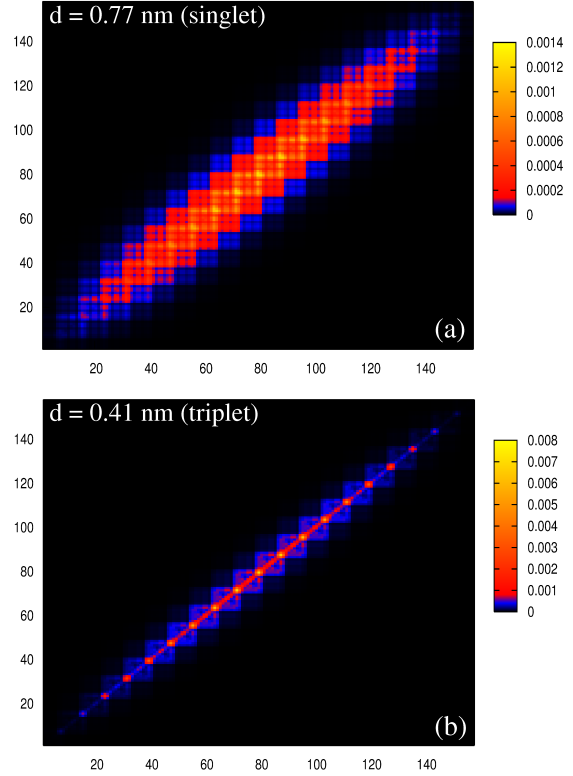


FIG. 1: (Color online) Probability density of the electron-hole separation (see text) in the (a) singlet and (b) triplet excitons of a 20-unit PPV chain (158 atoms) the atomic site indices. The rms electron-hole separation d is included in each case.

within Eq. (1) is to be expected. We postpone further discussion until later.

In Fig. 2, we show plots of $\rho_{ij}^{S(T)}$ for the (11,0) S-SWCNT, the (21,1) AGNR, and the (7,6) S-SWCNT. The (21,1) AGNR is obtained by “unrolling” the (11,0) NT, while the (7,6) NT has a diameter close to that of the (11,0) NT. These $\rho_{ij}^{S(T)}$ plots are representative for all other NTs and AGNRs, respectively. The probability density patterns are wider for all three carbon nanostructures compared to PPV, and are nearly the same for spin-singlet and triplet excitons. Both of these indicate some fundamental difference between the wave functions, in particular the triplet wave functions, in π -conjugated polymers versus the carbon nanostructures. The wider probability dispersion in the AGNR indicates greater electron-hole separation in the exciton wave functions here, presumably a consequence of partial two-dimensionality, as the exciton acquires greater width within the same unit cell. The $\rho_{ij}^{S(T)}$ for the (7,6) NT, with very large unit cells

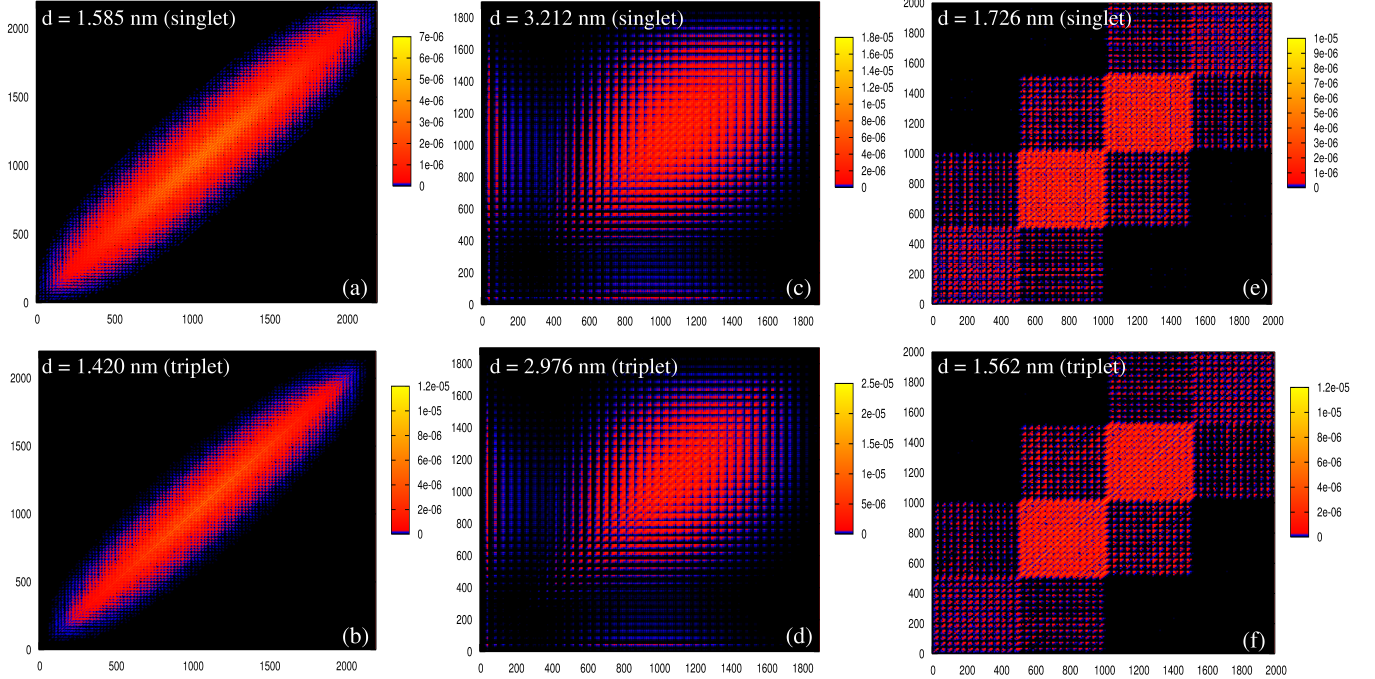


FIG. 2: (Color online) Probability density of the electron-hole separation in the lowest optical singlet exciton in (a) (11,0) S-SWCNT (50 unit cells, 2200 atoms), (c) (21,1) AGNR (40 unit cells, 1962 atoms) and (e) (7,6) S-SWCNT (4 unit cells, 2032 atoms). The probability densities of the electron-hole separation in the corresponding lowest triplet exciton are shown in (b), (d), and (f), respectively.

is particularly interesting. Each bright square within the checkerboard pattern in Figures 2(e) and (f) corresponds to i and j within the same unit cell. The overall pattern indicates exciton wave functions delocalized over the cylinder within a unit cell, even as the unit cells themselves are coupled one dimensionally (justifying partly the characterization of NTs as “quasi-one-dimensional”). Our results for *other chiral S-SWCNTs* also exhibit similar checkerboard patterns within the unit cell for $\rho_{ij}^{S(T)}$. Similar structure should be true also in the (11,0) zigzag NT, except that because of the much smaller unit cell size - 44 carbon atoms - this is not visible on the scale of Fig. 2. The wider dispersions of probability densities are consistent with the large $d_{S(T)}$ indicated in the figures. Our calculated $d_S \sim 1.5$ nm for the (6,5) NT is in excellent agreement with the experimental estimate of 2.0 ± 0.7 nm³⁸, giving us confidence in the accuracy of our method.

The confined versus delocalized behavior of excitons is clearly a dimensional effect. In order to understand this dimensional effect physically, we have performed systematic calculations of E_S and E_T for narrow AGNRs as functions of their widths (see Fig. 3). We start with a poly(p-phenylene) (PPP) chain as the narrowest AGNR with width

$W = a = 0.249$ nm, where a is the graphene unit lattice vector [Fig. 3(a)]. By adding more PPP chains on top of one another, we generate wider (1,1), (3,1), (4,1), and (6,1) AGNRs [(2,1) and (5,1) AGNRs are ignored as they are metallic]. A large decrease in Δ_{ST} , by ~ 0.9 eV between (1,1) and (3,1) AGNRs [see Fig. 3(b)] indicates the emergence of quasi-two-dimensional behavior already for the (3,1) AGNR. Interestingly, E_{bS} does not exhibit the sharp drop seen with Δ_{ST} and E_{bT} . Figure 3(c) shows the behavior of Δ_{ST} plotted against the inverse of the number of unit cells L in AGNRs. As seen here, Δ_{ST} has almost converged already at the smallest $L = 8$ for PPP and the (1,1) AGNR. For the wider AGNRs, however, Δ_{ST} continues to decrease with ribbon length even at the largest L for which we have done our calculations ($L = 60$). Figure 3(d) shows the corresponding behavior for $\eta = d_T/d_S$ as a function of W .

Let us now try to understand our main result, viz., $\Delta_{ST} \sim 0.1$ eV in S-SWCNTs with $d \sim 1$ nm. Δ_{ST} s even smaller than ours for S-SWCNTs of similar diameters were calculated in Refs. 2 and 3. The smaller Δ_{ST} was justified on the basis of the argument that it should be comparable to the energy splitting between optically bright and dark singlet

longitudinal excitons, which is, indeed, smaller than our Δ_{ST} ^{3,44}. These authors claimed that the bright-dark spin singlet exciton splitting is determined by the same exchange energy that gives the singlet-triplet splitting, and hence the two quantities should be comparable. This argument is not correct however. Bright-dark exciton splitting requires *pairs* of occupied orbitals (labeled, say, 1 and 2) and unoccupied orbitals (1' and 2'), such that within one-electron theory the optically allowed excited states $|1 \rightarrow 1'\rangle$ and $|2 \rightarrow 2'\rangle$ are nearly degenerate. In the presence of many-electron interactions that give nonzero matrix elements between these excited configurations new eigenstates $|1 \rightarrow 1'\rangle \pm |2 \rightarrow 2'\rangle$ are obtained of which one is optically bright and the other dark⁴⁵. Thus unlike in the exchange process where only two orbitals and two electrons are involved, permutation of the coordinates of pairs of electrons are not involved in the splitting behind the bright and dark excitons. The latter is thus driven by direct Coulomb interactions, as has also been emphasized by others⁴⁶. Both the direct and the exchange Coulomb interactions vary as $1/R$, where R is the exciton radius. The bright-dark splitting is small for the longitudinal excitons with large radii, but the same mechanism is behind the splitting of bright and dark *transverse* excitons in S-SWCNTs³⁵ and PPV³³, where because of the short radii of the transverse excitons, the Coulomb matrix elements are large and so are the splittings. The above argument justifies Δ_{ST} larger than the singlet bright-dark separation, as the exciton radii are smaller for the triplet than for the singlet exciton. In view of this and the results of Table I, we then arrive at the following interpretation of the experiments of Ref. 9: the optically dark states ~ 40 meV below the bright exciton are spin singlet, while the ones ~ 100 below are spin triplets. This interpretation agrees with our results for the triplets in Tables I and II.

Understanding the small Δ_{ST} in spite of the relatively large E_{bS} , in comparison to PPV, requires going through a somewhat more complicated discussion. The PPP Hamiltonian reduces in the strong-coupling limit to a Hubbard Hamiltonian [$V_{ij} = 0$ limit of Eq. (1)] with effective U , $U_{\text{eff}} \simeq U - V_{12}$, where V_{12} is the nearest-neighbor repulsion. The correlated-electron wave function of π -conjugated polymers corresponds to that of a Mott-Hubbard semiconductor, since in one dimension the critical U (hereafter U_c) for metal-insulator transition within the simple Hubbard model is arbitrarily small⁴⁷. This implies that the ground state is dominated by covalent valence bond diagrams with only singly occupied sites⁴⁸. *The important point now is that the nature of the ground-state wave function and of the*

lowest spin triplet states are related. Thus the lowest triplet states in one dimension are also covalent, while the optical state consists of ionic valence bond diagrams⁴⁸. This is why of course Δ_{ST} in π -conjugated polymers is large.

In contrast to one dimension, recent theoretical work has shown that in the graphene lattice U_c is rather large, $U_c \geq 4t_{ij}$ ⁴⁹. Graphene is a semimetal since U_{eff} within the PPP model is smaller than this U_c . It is likely that U_c becomes nonzero for nanoribbons with finite width W_c , with U_c rising gradually with width $W > W_c$. For nanoribbons that are metallic within one-electron theory and have $W > W_c$ then the ground-state wave function is no longer covalent but has strong admixing with ionic configurations with double occupancies. We *speculate* that a similar effect occurs in *semiconducting* nanoribbons with $W > W_c$, where the ground-state wave function begins to resemble that of a conventional semiconductor rather than a Mott-Hubbard semiconductor. This would also mean that the ground state is no longer covalent; furthermore, in conventional semiconductors, the singlet optical state and the triplet are both ionic and Δ_{ST} is small. Our calculations in Fig. 3(b) then suggest that $W_c \sim 2.5a$. Although we have presented the above arguments above for the AGNRs only, it is clear that they also apply to S-SWCNTs. The remaining problem now is to understand the large E_{bS} in the S-SWCNTs and AGNRs in spite of small Δ_{ST} .

The exciton binding energy unlike Δ_{ST} is largely unrelated to the nature of the ground state, as both the exciton and the electron-hole continuum states are ionic within valence bond theory for all U_{eff} . Hence E_{bS} is given by the intersite interaction V_{ij} between a particle (double occupancy) and a hole (vacancy) within the effective Hubbard Hamiltonian, and small Δ_{ST} does not preclude large E_{bS} . A direct demonstration of all of the above (especially the existence of a W_c) is beyond the scope of our current work. However, large E_{bS} in spite of small Δ_{ST} within Eq. (1) can be demonstrated easily. In Fig. 4, we show our calculated E_{bS} and Δ_{ST} within Eq. (1) for a hypothetical PPV chain with fixed U but varying κ . Smaller κ implies larger V_{ij} and smaller U_{eff} . The behavior of E_{bS} and Δ_{ST} against κ are exactly opposite, E_{bS} increases while Δ_{ST} decreases with increasing V_{ij} .

IV. CONCLUSIONS

To summarize, beyond a critical diameter in S-SWCNTs and width in AGNRs, Δ_{ST} decreases rapidly with further increase in diameter or width.

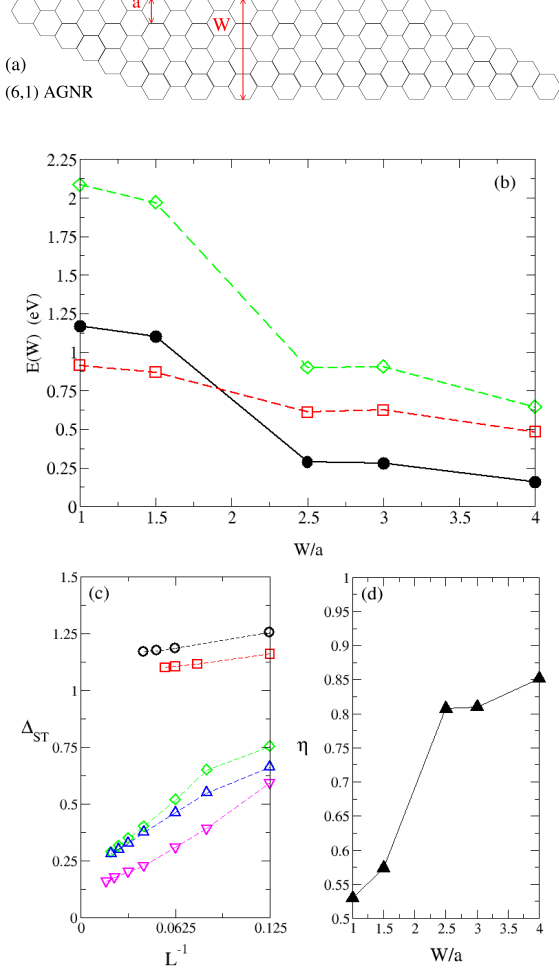


FIG. 3: (Color online) (a) Fragment of a (6,1) AGNR with width $W = 4a$, where $a = 0.249$ nm is the graphene unit lattice vector. (b) Δ_{ST} (filled circle), E_{bs} (open square), and E_{bT} (open diamond) as functions of W . (c) Δ_{ST} vs the inverse of the number of unit cells L for PPP (circle), (1,1) (square), (3,1) (diamond), (4,1) (triangle up), and (6,1) (triangle down) AGNRs. (d) Ratio $\eta = d_T/d_S$ as a function of W .

Our results for Δ_{ST} are intermediate between the very small values in Refs. 2 and 3 and the much larger values in Ref. 4. In S-SWCNTs with $d \sim 1$ nm, and in AGNRs with comparable widths, Δ_{ST} is nearly an order of magnitude smaller than in one-dimensional conjugated polymers. Δ_{ST} in S-SWCNTs is smaller than the splitting between bright and dark spin-singlet excitons. Furthermore, there is no one-to-one correspondence between the exciton binding energy and the singlet-triplet splitting, and small Δ_{ST} does not preclude moderately large exciton binding energy.

The small Δ_{ST} in wide S-SWCNTs and AGNRs

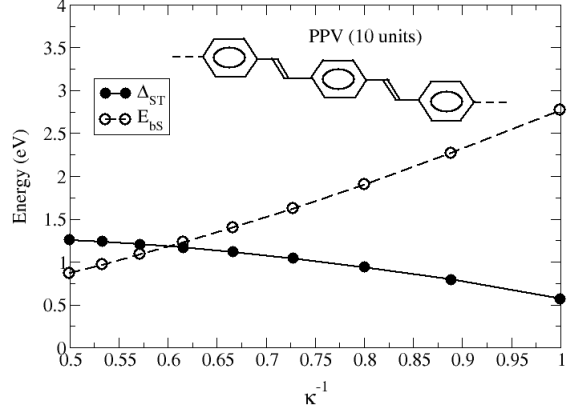


FIG. 4: Δ_{ST} (solid line with filled circle) vs E_{bs} (dashed line with open circle) as a function of κ^{-1} for a PPV chain with 10 units.

may have interesting practical applications in the area of organic photovoltaics. Carbon-based excitonic solar cells consist of type II heterostructures with donor and acceptor molecular systems. Optical excitation of the donor, followed by photoinduced charge-transfer from the donor to the acceptor, lie at the heart of the device operation here. The exciton diffusion wavelength is usually quite short, and so is the singlet exciton lifetime. As a consequence, there is considerable loss in efficiency due to the singlet exciton relaxing to the ground state before it reaches the donor-acceptor interface. One way to enhance the performance is to utilize the spin-triplet exciton with a longer lifetime than the singlet exciton. Our theoretical results for Δ_{ST} in carbon nanostructures here are interesting in this context, since ISC in systems with small Δ_{ST} is expected to be rapid and efficient. Enhanced photoinduced charge-transfer from the spin-triplet exciton in S-SWCNTs and AGNRs to acceptor molecules is therefore a distinct possibility. While early attempts to construct solar cells with S-SWCNTs as acceptors did not lead to encouraging results^{50–55}, impressive performance in blends of S-SWCNTs with $d \sim 1$ nm and C_{60} , with S-SWCNTs as the donor materials has been obtained^{56,57}. Spin-triplet participation may be behind this dramatic improvement.

V. ACKNOWLEDGMENTS

We are grateful to S. Tretiak for useful discussions. This work was partially supported by US NSF

- ¹ A. Jorio, G. Dresselhaus, and M. S. Dresselhaus, *Carbon Nanotubes: Advanced Topics in the Synthesis, Structure, Properties and Applications* (Springer-Verlag, New York, LLC, 2008).
- ² V. Perebeinos, J. Tersoff, and P. Avouris, *Nano Lett.* **5**, 2495 (2005).
- ³ R. B. Capaz, C. D. Spataru, S. Ismail-Beigi, and S. G. Louie, *Phys. Stat. Solidi (b)* **244**, 5016 (2007).
- ⁴ S. Tretiak, *Nano Lett.* **7**, 2201 (2007).
- ⁵ A. D. Mohite, T. S. Santos, J. S. Moodera and B. W. Alphenaar, *Nat. Nanotechnology* **4**, 425 (2009).
- ⁶ I. B. Mortimer, L. J. Li, R. A. Taylor, G. L. J. A. Rikken, O. Portugall, and R. J. Nicholas, *Phys. Rev. B* **76**, 085404 (2007).
- ⁷ I. B. Mortimer, and R. J. Nicholas, *Phys. Rev. Lett.* **98**, 027404 (2007).
- ⁸ J. Shaver, J. Kono, O. Portugall, V. Krstic, G. L. J. A. Rikken, Y. Miyauchi, S. Maruyama, and V. Perebeinos, *Nano Lett.* **7**, (7) 1851 (2007).
- ⁹ O. Kiowski, K. Arnold, S. Lebedkin, F. Hennrich, and M. M. Kappes, *Phys. Rev. Lett.* **99**, (23) 237402 (2007).
- ¹⁰ A. Srivastava, H. Htoon, V. I. Klimov, and J. Kono, *Phys. Rev. Lett.* **101**, (8) 087402 (2008).
- ¹¹ R. Matsunaga, K. Matsuda, and Y. Kanemitsu, *Phys. Rev. Lett.* **101**, (14) 147404 (2008).
- ¹² R. Matsunaga, K. Matsuda, and Y. Kanemitsu, *J. Lumin.* **129**, (12) 1702 (2009).
- ¹³ H. Harutyunyan, T. Gokus, A. A. Green, M. C. Hersam, M. Allegrini, and A. Hartschuh, *Nano Lett.* **9**, 2010 (2009).
- ¹⁴ K. Nagatsu, S. Chiashi, S. Konabe and Y. Homma, *Phys. Rev. Lett.* **105**, 157403 (2010).
- ¹⁵ R. Matsunaga, K. Matsuda, and Y. Kanemitsu, *Phys. Rev. B* **81**, 033401 (2010).
- ¹⁶ L. Yang, M. L. Cohen, and S. G. Louie, *Nano Lett.* **7**, 3112 (2007).
- ¹⁷ L. Yang, C.-H. Park, Y.-W. Son, M. L. Cohen, and S. G. Louie, *Phys. Rev. Lett.* **99**, 186801 (2007).
- ¹⁸ D. Prezzi, D. Varsano, A. Ruini, A. Marini, and E. Molinari, *Phys. Rev. B* **77**, 041404(R) (2008).
- ¹⁹ W. H. Liao, G. G. Zhou, and F. Xi, *J. Appl. Phys.* **104**, 126105 (2008).
- ²⁰ K. Gundra, and A. Shukla, *Phys. Rev. B* **83**, 075413 (2011).
- ²¹ Y. Cao, I. D. Parker, G. Yu, C. Zhang, and A. J. Heeger, *Nature (London)* **397**, 414 (1999).
- ²² J.-S. Kim, K. H. P. Ho, N. C. Greenham, and R. H. Friend, *J. Appl. Phys.* **88**, 1073 (2000).
- ²³ M. Wohlgenannt, K. Tandon, S. Mazumdar, S. Ramasesha, and Z. V. Vardeny, *Nature (London)* **409**, 494 (2001).
- ²⁴ K. Tandon, S. Ramasesha and S. Mazumdar, *Phys. Rev. B* **67**, 045109 (2003).
- ²⁵ A. S. Dhoot, D. S. Ginger, D. Beljonne, Z. Shuai, N. C. Greenham, *Chem. Phys. Lett.* **360**, 195 (2002).
- ²⁶ M. Segal, M. A. Baldo, R. J. Holmes, S. R. Forrest, and Z. G. Soos, *Phys. Rev. B* **68**, 075211 (2003).
- ²⁷ M. Carvelli, R. A. J. Janssen, and R. Coehoorn, *Phys. Rev. B* **83**, 075203 (2011).
- ²⁸ M. Arif, K. Yang, K. Li, P. Yu, S. Guha, S. Gangopadhyay, M. Förster, and U. Scherf, *Appl. Phys. Lett.* **94**, 063307 (2009).
- ²⁹ M. B. Smith, and J. Michl, *Chem. Rev.* **110**, 6891 (2010).
- ³⁰ A. P. Monkman, H. D. Burrows, L. J. Hartwell, M. da G. Miguel, I. Hamblett, and S. Navaratnam, *Chem. Phys. Lett.* **307**, 303 (1999).
- ³¹ R. Pariser, and R. G. Parr, *J. Chem. Phys.* **21**, 466 (1953).
- ³² J. A. Pople, *Trans. Faraday Soc.* **49**, 1375 (1953).
- ³³ M. Chandross, and S. Mazumdar, *Phys. Rev. B* **55**, 1497 (1997).
- ³⁴ Z. Wang, H. Zhao, and S. Mazumdar, *Phys. Rev. B* **74**, 195406 (2006).
- ³⁵ Z. Wang, H. Zhao, and S. Mazumdar, *Phys. Rev. B* **76**, 115431 (2007).
- ³⁶ K. Ohno, *Theor. Chim. Acta.* **2**, 219 (1964).
- ³⁷ M. Ezawa, *Phys. Rev. B* **73**, 045432 (2006).
- ³⁸ L. Lüer, S. Hoseinkhani, D. Polli, J. Crochet, T. Hertel, and G. Lanzani, *Nat. Phys.* **5**, 54 (2009).
- ³⁹ G. Dukovic, F. Wang, D. Song, M. Y. Sfeir, T. F. Heinz, and L. E. Brus, *Nano Lett.* **5**, 2314 (2005).
- ⁴⁰ H. Zhao, S. Mazumdar, C.-X. Sheng, M. Tong, and Z. V. Vardeny, *Phys. Rev. B* **73**, 075403 (2006).
- ⁴¹ S. M. Bachilo, M. S. Strano, C. Kittrell, R. H. Hauge, R. E. Smalley, and R. B. Weisman, *Science*, **298**, 2361 (2002).
- ⁴² A. Köhler, and D. Beljonne, *Adv. Func. Mater.* **14**, 11 (2004).
- ⁴³ D. Beljonne, J. Cornil, R. H. Friend, R. A. J. Janssen, and J. L. Brédas, *J. Am. Chem. Soc.* **118**, 6453 (1996).
- ⁴⁴ C. D. Spataru, S. Ismail-Beigi, R. B. Capaz, and S. G. Louie, *Phys. Rev. Lett.* **95**, 247402 (2005).
- ⁴⁵ H. Zhao, and S. Mazumdar, *Phys. Rev. Lett.* **93**, 157402 (2004).
- ⁴⁶ E. Chang, D. Prezzi, A. Ruini, and E. Molinari, eprint arXiv:cond-mat/0603085v1 (unpublished).
- ⁴⁷ E. H. Lieb, and F. Y. Wu, *Phys. Rev. Lett.* **20**, 1445 (1968).
- ⁴⁸ S. Ramasesha, and Z. G. Soos, *J. Chem. Phys.* **80**, 3278 (1984).
- ⁴⁹ Z. Y. Meng, T. C. Lang, S. Wessel, F. F. Assaad, and A. Muramatsu, *Nature (London)* **464**, 847 (2010).
- ⁵⁰ S. Kazaoui, N. Minami, B. Nalini, Y. Kim, and K. Hara, *J. Appl. Phys.* **98**, (8) 084314 (2005).
- ⁵¹ E. Kymakis, and G. A. J. Amaratunga, *Rev. Adv. Mater. Sci.* **10**, (4) 300 (2005).

- ⁵² V. Sgobba, G. M. A. Rahman, D. M. Guldi, N. Jux, S. Campidelli, and M. Prato, *Adv. Mater.* **18**, (17) 2264 (2006).
- ⁵³ T. Hasobe, S. Fukuzumi, and P. V. Kamat, *J. phys. chem. B* **110**, (50) 25477 (2006).
- ⁵⁴ Y. Kanai, and J. C. Grossman, *Nano Lett.* **8**, (3) 908 (2008).
- ⁵⁵ B. J. Landi, R. P. Raffaele, S. L. Castro, and S. G. Bailey, *Prog. Photovoltaics* **13**, (2) 165 (2005).
- ⁵⁶ M. S. Arnold, J. D. Zimmerman, C. K. Renshaw, X. Xu, R. R. Lunt, C. M. Austin, and S. R. Forrest, *Nano Lett.* **9**, 3354 (2009).
- ⁵⁷ D. J. Bindl, W. Meng-Yin, F. C. Prehn, M. S. Arnold, *Nano Lett.* **11**, 455 (2011).